PNAS RESEARCH ARTICLE | GENETICS

Neuronal MML-1/MXL-2 regulates systemic aging via glutamate transporter and cell nonautonomous autophagic and peroxidase activity

Tatsuya Shioda[a], Ittetsu Takahashi[a], Kensuke Ikenaka[b], Naonobu Fujita[c,d], Tomotake Kanki[e], Toshihiko Oka[f], Hideki Mochizuki[b], Adam Antebi[g,h], Tamotsu Yoshimori[a,i,j,1], and Shuhei Nakamura[a,i,k,1,2]

Edited by Ana Maria Cuervo, Albert Einstein College of Medicine, New York, NY; received December 20, 2022; accepted August 4, 2023

Accumulating evidence has demonstrated the presence of intertissue-communication regulating systemic aging, but the underlying molecular network has not been fully explored. We and others previously showed that two basic helix–loop–helix transcription factors, MML-1 and HLH-30, are required for lifespan extension in several longevity paradigms, including germlineless *Caenorhabditis elegans*. However, it is unknown what tissues these factors target to promote longevity. Here, using tissue-specific knockdown experiments, we found that MML-1 and its heterodimer partners MXL-2 and HLH-30 act primarily in neurons to extend longevity in germlineless animals. Interestingly, however, the downstream cascades of MML-1 in neurons were distinct from those of HLH-30. Neuronal RNA interference (RNAi)-based transcriptome analysis revealed that the glutamate transporter GLT-5 is a downstream target of MML-1 but not HLH-30. Furthermore, the MML-1-GTL-5 axis in neurons is critical to prevent an age-dependent collapse of proteostasis and increased oxidative stress through autophagy and peroxidase MLT-7, respectively, in long-lived animals. Collectively, our study revealed that systemic aging is regulated by a molecular network involving neuronal MML-1 function in both neural and peripheral tissues.

longevity | autophagy | redox homeostasis | *C. elegans*

Significance

The Mondo complex (MML-1/MXL-2) is required for multiple longevity-promoting pathways in *Caenorhabditis elegans.* However, the tissues involved in this function of MML-1/MXL-2 have remained elusive. Here, we found that neuronal MML-1/MXL-2 was preferentially involved in the longevity and maintenance of tissue integrity conferred by germline deficiency. Neuronal MML-1/MXL-2 activated transcription of the glutamate transporter *glt-5,* which modulated autophagic activity and redox homeostasis by increasing expression of the peroxidase *mlt-7* in nonneuronal tissues of long-lived animals. Our study provides evidence that intertissue-communications by neuronal MML-1/MXL-2 result in systemic regulation that is crucial for controlling organismal aging.

Aging has long been thought to be an uncontrollable event attributed to a passive increase in entropy over time. This hypothesis was refuted by the discovery of conserved signaling pathways that extend lifespan, including reduced insulin/insulin growth factor-1 signaling (IIS), dietary restriction, reduced target of rapamycin (TOR) signaling, reduced mitochondrial respiration, and germline removal (1, 2). Interestingly, although these pathways partially share certain features, they basically constitute independent transcriptional regulatory networks that regulate proteostasis, stress resistance, redox homeostasis, metabolism, and immunity, thereby extending lifespan. For instance, in *Caenorhabditis elegans* (*C. elegans*) studies, it has been reported that IIS-mediated longevity requires the activities of several transcription factors, including DAF-16/FOXO, HSF-1, and SKN-1/NRF2 (3–5). On the other hand, longevity via dietary restriction depends on SKN-1, PHA-4/FOXA, and NHR-62/HNF4, but not DAF-16 or HSF-1 (5–9).

There is mounting evidence that several transcription factors act in specific organs to extend lifespan. For example, DAF-16 activity in neurons and the intestine are required for IIS-mediated longevity (10, 11). In addition, activation of XBP-1 (X-box binding protein 1) in neurons was found to be sufficient to induce the neuronal endoplasmic reticulum (ER) unfold protein response (UPR^{ER}) to coordinate systemic aging (12–14). Furthermore, neuronal overexpression of the canonical heat shock transcription factor, HSF-1, significantly increased heat stress tolerance and lifespan in wild-type (WT) animals (15). Further characterization of the tissue specificities of these transcription factors and identification of the role of intertissue-signaling in lifespan extension will help elucidate the complex mechanism of aging at the organismal level.

The Myc superfamily basic helix–loop–helix (bHLH) transcription factor MML-1 (Myc and Mondo-like 1) and its heterodimer partner MXL-2 (MAX-like 2) have recently been identified as modulators of longevity conferred by germline removal (16). In animals with germline deficiency, the MML-1/MXL-2 complex was translocated to the nucleus in cells throughout the body and contributed to lifespan extension by inducing autophagic activity, an evolutionally conserved intracellular bulk degradation system. Additionally, MML-1/MXL-2 knockdown impaired the nuclear localization and activation of bHLH transcription factor EB (TFEB), a master regulator of autophagy, lysosome biogenesis, and lipid catabolism in germlineless long-lived *glp-1* mutants, and vice versa (17–19). Of note, the functions of MML-1/MXL-2 and HLH-30, in addition to the downstream

Author contributions: T.S. and S.N. designed research; T.S., I.T., K.I., and S.N. performed research; N.F., T.K., T.O., H.M., and A.A. contributed new reagents/analytic tools; T.S. analyzed data; T.S. funding acquisition; T.Y. and S.N. project administration and funding acquisition; and T.S., T.Y., and S.N. wrote the paper.

Competing interest statement: T.Y. and S.N. are founders of AutoPhagyGO.

This article is a PNAS Direct Submission.

[1]To whom correspondence may be addressed. Email: tamyoshi@fbs.osaka-u.ac.jp or shuhei.nakamura@naramed-u.ac.jp.

[2]Present address: Department of Biochemistry, Nara Medical University, Kashihara 634-8521, Japan.

This article contains supporting information online at https://www.pnas.org/lookup/suppl/doi:10.1073/pnas.2221553120/-/DCSupplemental.

Published September 18, 2023.

autophagic activity, were also required for the longevity by reduced insulin/IGF-I, reduced TOR signaling, dietary restriction reduced mitochondrial respiration in addition to germline removal (16, 20, 21). This suggests that MML-1 and HLH-30 are convergent transcriptional regulators in multiple longevity pathways. Nevertheless, the tissue-specific roles of MML-1 and HLH-30 in extending lifespan remain largely unknown.

In this study, we investigated how MML-1/MXL-2 and HLH-30 in different tissues contributed to lifespan extension. Using tissue-specific RNAi systems in *C. elegans*, we identified that neuronal MML-1/MXL-2 and HLH-30 played a critical role in longevity. Importantly, transcriptome analysis revealed that neuronal MML-1/MXL-2 targets a different set of genes than neuronal HLH-30. Moreover, neuronal MML-1/MXL-2 up-regulated the expression of the glutamate transporter GLT-5 in neurons, resulting in enhanced autophagic and peroxidase MLT-7 activity in peripheral tissues, which ultimately prolonged lifespan. Our findings show that neuronal MML-1/MXL-2 is a modulator of systemic aging that functions via autophagic activation and the maintenance of redox homeostasis.

Results

Neuronal MML-1/MXL-2 Is Required for the Longevity of Germlineless Animals. To determine the critical tissue in which MML-1 and its heterodimer partner, MXL-2, contribute to extending lifespan, we conducted tissue-specific knockdown of *mml-1* and *mxl-2* and examined their effect on the longevity of germlineless *glp-1* mutants. To do this, we crossed germlineless *glp-1* mutants with strains sensitive to RNAi of specific tissues, including TU3401 (neurons), VP303 (intestine), NR222 (hypodermis), and NR350 (muscle) (22–24). We found that neuronal or hypodermal suppression of *mml-1* completely abolished the longevity of *glp-1* mutants (Fig. 1*A* and *SI Appendix*, Fig. S1*A*). On the contrary, neither intestine- nor muscle-specific *mml-1* knockdown affected *glp-1* longevity (*SI Appendix*, Fig. S1 *B* and *C*). We also found that knockdown of *mxl-2* in neurons abolished *glp-1* longevity (Fig. 1*B*), while intestine-, hypodermis-, or muscle-specific inhibition had little or no effect (*SI Appendix*, Fig. S1 *D–F*). These results suggest that the neuronal MML-1/MXL-2 complex preferentially plays a role in *glp-1* longevity.

The evolutionarily conserved IIS is one of the best-characterized pathways involved in regulating lifespan (3, 25, 26). Given that the MML-1/MXL-2 complex is implicated in lifespan extension mediated by several pathways, including IIS (16), we asked whether neuronal MML-1/MXL-2 also contributes to IIS-dependent longevity. As expected, neuronal *mml-1* or *mxl-2* suppression significantly abolished *daf-2* longevity (Fig. 1 *C* and *D*), suggesting critical roles for neuronal MML-1/MXL-2 in IIS-mediated longevity, as in *glp-1* longevity. Furthermore, worms expressing *mml-1* under the panneuronal *rab-3p* promoter showed an extended median lifespan (Fig. 1*E*) (27). Altogether, these findings indicate that neuronal MML-1/MXL-2 plays a crucial role in prolonging the lifespan of *C. elegans*.

In previous studies, several transcription factors that were shown to regulate longevity contributed to lifespan extension during a specific period rather than throughout an organism's lifetime (28–31). However, the temporal requirements of MML-1 for longevity were unknown. To address this, we conducted neuronal knockdown of *mml-1* in *glp-1* mutants in different stages of adulthood and found that neuronal MML-1 during early life was predominantly required for *glp-1* longevity (Fig. 1*F*).

Our tissue-specific analysis revealed the critical role of neuronal MML-1/MXL-2 in lifespan regulation, we investigated whether these genes are expressed in neurons. Using WormSeq, a web interface that enables easy exploration of the whole-body transcriptional landscape of the adult *C. elegans* (32), we found that *mml-1/mxl-2* was widely expressed in a variety of neuronal cells (*SI Appendix*, Fig. S1 *G* and *H*). We then used MML-1::GFP (Green Fluorescent Protein) transgenic worms and analyzed the MML-1::GFP nuclear enrichment upon germline deficiency. Importantly, nuclear MML-1::GFP was drastically increased in nerve-ring neurons of *glp-1* mutants compared with WT animals (Fig. 1 *G* and *H*), indicating that germline deficiency provokes nuclear translocation of MML-1 in neurons. These data provide evidence in support of an important role for neuronal MML-1/MXL-2 in lifespan extension.

Neuronal HLH-30/TFEB Is Also Essential for the Longevity of *glp-1* Mutants. HLH-30, the *C. elegans* homolog of TFEB, is translocated to the nucleus by germline removal and contributes to longevity by up-regulating autophagy and lysosomal gene expression (21, 33). Notably, we have previously shown that MML-1 and HLH-30 mutually regulate each other's activities in germlineless animals (16). Therefore, we tested the hypothesis that HLH-30 also acts in neurons to regulate *glp-1* longevity. Indeed, we found that suppression of *hlh-30* in neurons partially abolished *glp-1* longevity (*SI Appendix*, Fig. S2*A*), while targeting *hlh-30* in the intestine, hypodermis, or muscle had little impact (*SI Appendix*, Fig. S2 *B–D*). We confirmed that adult only *hlh-30* RNAi significantly suppresses the endogenous HLH-30::mNeonGreen in each tissue in all tissue-specific knockdown strains within 4 d (*SI Appendix*, Fig. S2 *F–M*). Interestingly, unlike *mml-1*, knockdown of neuronal *hlh-30* from day 5 or day 10 of adulthood suppressed *glp-1* longevity to the same level as when it was suppressed from day 1 (*SI Appendix*, Fig. S2*E*). Taken together, these results suggest that neuronal *hlh-30,* as well as *mml-1/mxl-2* has an important role in the longevity of germline-deficient animals.

The effect of *hlh-30* overexpression in neurons was then examined in WT worms, and those expressing *rab-3p::hlh-30* did not exhibit an increased lifespan (*SI Appendix*, Fig. S2*N*). As with MML-1/MXL-2, therefore, neuronal HLH-30 is required for *glp-1* longevity, but unlike MML-1, HLH-30 overexpression in neurons is not sufficient to prolong lifespan.

Neuronal Suppression of *mml-1/mxl-2* Accelerates Aging-Associated Phenotypes. We next evaluate the effects of neuronal knockdown of *mml-1*, *mxl-2*, and *hlh-30* on several aging-associated phenotypes. Intestinal autofluorescence caused by lipofuscin accumulation increases with age and is often used as a marker of aging (34–36). Germline removal attenuated the age-related increase in intestinal autofluorescence (*SI Appendix*, Fig. S3 *A* and *B*). However, this beneficial effect was abolished by neuronal suppression of *mml-1*, *mxl-2,* or *hlh-30*. Next, we used a multiworm tracking (MWT) system that enabled the tracking of individual worms to calculate their movement speeds on nematode growth medium (NGM) plates (37) to test the effect of them on locomotion activity. Inhibition of neuronal *mml-1* or *mxl-2* significantly reduced the motility of *glp-1* mutants compared to control worms, whereas neuronal knockdown of *hlh-30* did not (*SI Appendix*, Fig. S3 *C* and *D*). Recent studies have shown that intestinal integrity is disrupted with aging in a variety of organisms (38, 39). To verify their influence on intestinal integrity, we assessed the leakage of blue food dye from the intestine (animals exhibiting this leakage are referred to as having the "Smurf" phenotype) (39). While the incidence of the Smurf phenotype increased with age in WT animals, it was significantly lower in germline-deficient animals (*SI Appendix*, Fig. S3 *E* and *F*). Notably, the intestinal

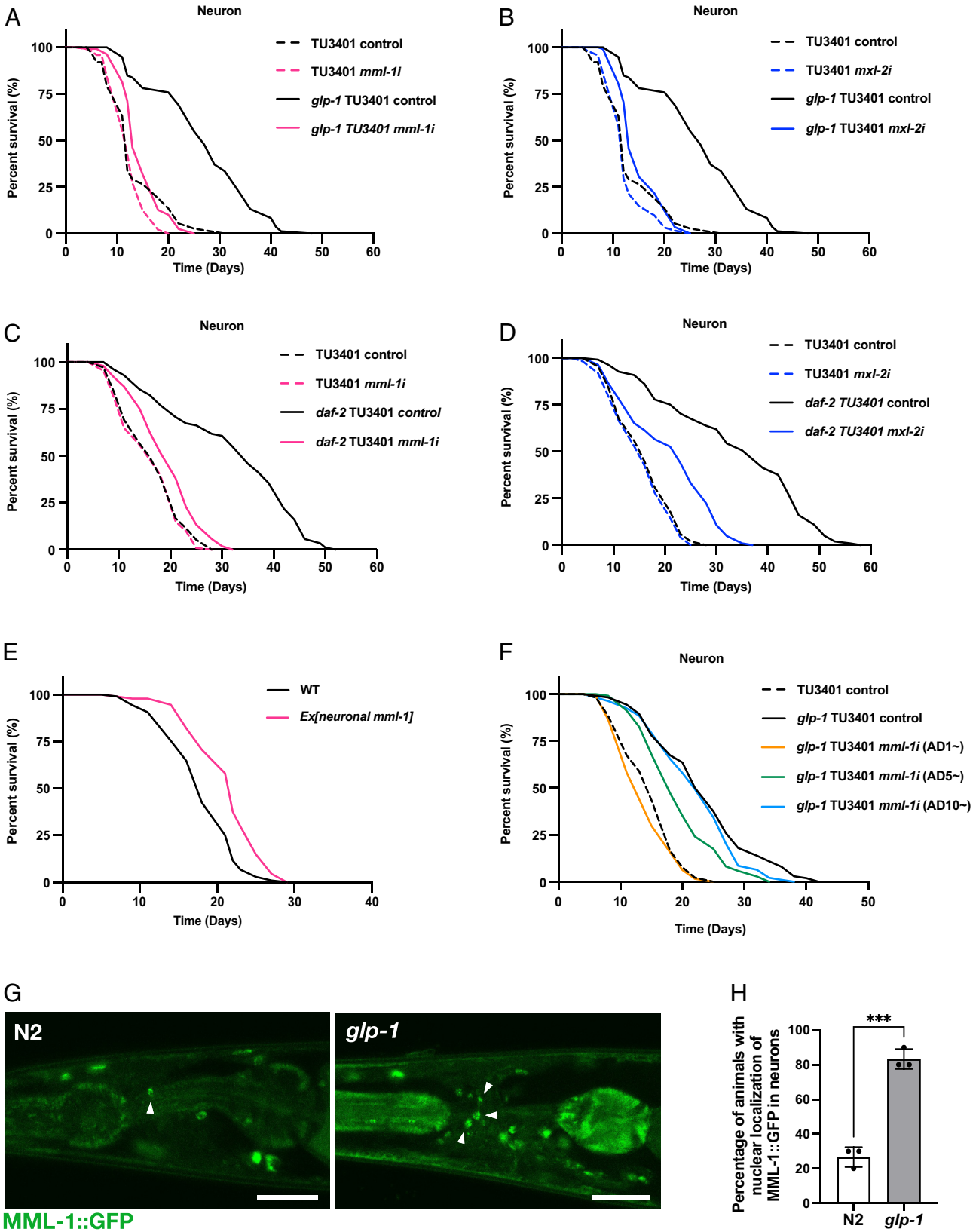

Fig. 1. Neuronal MML-1/MXL-2 is involved in the regulation of lifespan. (*A*) Neuronal knockdown of *mml-1* suppressed the longevity of germline-deficient *glp-1(e2141)* mutants. TU3401 (a neuronal RNAi-sensitive strain) was used and knockdown was conducted from adult day 1. Representative data from three independent experiments are shown. See *SI Appendix*, Table S2 for details and repeats. (*B*) Neuronal *mxl-2* was required for *glp-1(e2141)* longevity. Knockdown was conducted from adult day 1. (*C*) Suppression of neuronal *mml-1* also abolished the longevity of IIS-deficient *daf-2(e1370)* mutants. Knockdown was conducted from adult day 1. (*D*) Neuronal *mxl-2* was also essential for *daf-2(e1470)* longevity. Knockdown was conducted from adult day 1. (*E*) Neuronal *mml-1* overexpression (*rab-3p::mml-1::gfp*) extended median lifespan in WT animals (20 °C). (*F*) Lifespans of *glp-1* mutants after neuronal *mml-1* knockdown from adult day 1 (AD1~), 5 (AD5~), or 10 (AD10~). Suppression of neuronal *mml-1* after day 5 or 10 shows little effect on the longevity of *glp-1* mutants compared to that of knockdown on day 1. (*G*) The representative fluorescent images of MML-1::GFP transgenic worms in nerve-ring neurons of WT N2 and *glp-1* worms at day 1 young adult stage. (*H*) Quantification of nuclear MML-1::GFP in nerve-ring neurons at day 1 young adult stage. Values represent mean ± SD from three biological replicates (10 worms each). *P* values (***$P < 0.001$) were determined by *t* test. (Scale bars, 20 μm [*G*].)

integrity of *glp-1* mutants was reduced by inhibition of neuronal *mml-1* or *mxl-2*. In addition, suppression of neuronal *hlh-30* also tended to increase the Smurf phenotype, although not statistically significant. Taken together, we found that neuronal suppression of these genes, especially *mml-1* and *mxl-2*, accelerated several aging-associated phenotypes.

Neuronal MML-1/MXL-2 Is Essential for Autophagic Activity in Long-Lived Animals. Autophagy is an evolutionally conserved intracellular degradation process whose activation is essential for several longevity pathways, including germline longevity (20, 40–43). A previous study revealed that MML-1/MXL-2 regulates autophagy essential for germline longevity (16). Since neuronal MML-1/MXL-2 was required for longevity in *glp-1*, we wondered if neuronal MML-1/MXL-2 also affects autophagy in specific tissues. Since germline deficiency increases the expression of autophagy-related (*atg*) genes (42), we first asked whether neuronal MML-1/MXL-2 regulates systemic ATG gene transcription. Neuronal suppression of *mml-1/mxl-2* did not result in significant differences in ATG genes transcription (*SI Appendix*, Fig. S4 *A–H*), although it slightly tended to alter the expression of these genes. Then, to determine if neuronal MML-1/MXL-2 contributes to autophagy in *glp-1* mutants, we performed an autophagy flux assay in *glp-1* mutants by treatment of autophagy inhibitor chloroquine, which blocks autophagosome fusion with lysosomes and quantified the numbers of autophagosomes labeled by GFP::LGG-1 in several tissues (40, 44). We observed an increased number of GFP::LGG-1 punctae in nerve-ring neurons of *glp-1* mutants after chloroquine treatment (Fig. 2 *A* and *B*). However, when neuronal *mml-1* or *mxl-2* was suppressed, chloroquine treatment did not significantly increase the number of GFP::LGG-1 punctae in neurons compared to control worms. Interestingly, we found that neuronal RNAi of *mml-1/mxl-2* also reduced autophagy flux in the intestine (Fig. 2 *C* and *D*) and muscle (Fig. 2 *E* and *F*). These results indicate that neuronal suppression of *mml-1/mxl-2* decreases the autophagy flux in several tissues.

Aggregates of polyglutamine (polyQ) proteins, which are involved in Huntington's disease and other neurodegenerative disorders, are one of the substrates degraded by autophagy (45–47). To verify whether neuronal MML-1/MXL-2 contributes to autophagic clearance of polyQ aggregates in distal tissue, we utilized worms expressing YFP-tagged polyQ in body-wall muscle. Suppression of neuronal *mml-1/mxl-2* reversed the effect of reduced polyQ aggregation caused by germline loss (Fig. 2 *G* and *H*). This result provides further evidence that neuronal MML-1/MXL-2 regulates muscle autophagy. Of note, longevity mediated by overexpression of neuronal MML-1 was completely abolished by systemic RNAi of an essential autophagy regulator, *bec-1/Beclin1* (Fig. 2*I*). Given the lack of neuronal response to systemic RNAi (24, 48), this finding indicates that autophagic activity in tissues other than neurons is required for the longevity conferred by neuronal MML-1 overexpression. These results suggest that neuronal MML-1/MXL-2 contributes to extending lifespan by modulating autophagic activity in several tissues.

Neuronal MML-1/MXL-2 and HLH-30 Control Independent Downstream Targets. To better understand how neuronal MML-1 and MXL-2 contribute to *glp-1* longevity, we next conducted RNA sequencing (RNA-seq) analysis and compared transcriptomes of WT control worms (TU3401 control), control worms lacking germline (*glp-1* TU3401 control), and *glp-1* mutants with neuronal knockdown of *mml-1* (*glp-1* TU3401 *mml-1i*), *mxl-2* (*glp-1* TU3401 *mxl-2i*), or *hlh-30* (*glp-1* TU3401 *hlh-30i*). Control worms lacking germline differentially expressed 14,732 transcripts compared to WT control worms of these transcripts, 87 and 78 were regulated by neuronal *mml-1* and *mxl-2* in the *glp-1* background, respectively (*SI Appendix*, Fig. S5*A* and Dataset S1). Notably, of the 87 transcripts regulated by neuronal *mml-1*, 51 were shared with neuronal *mxl-2*. Surprisingly, almost all transcripts regulated by neuronal *hlh-30* in *glp-1* mutants were independent of neuronal *mml-1* and *mxl-2* (*SI Appendix*, Fig. S5*B* and Dataset S1), suggesting that neuronal HLH-30 contributes to lifespan extension via downstream pathway distinct from neuronal MML-1 and MXL-2.

Gene Ontology (GO) analysis of up- or down-regulated genes in *glp-1* mutants with neuronal *mml-1/mxl-2* knockdown compared with *glp-1* worms revealed the enrichment of common biological processes, including UDP-glycosyltransferase activity, fatty acid degradation, oxidation-reduction processes, and carbohydrate metabolic processes (*SI Appendix*, Fig. S5 *C* and *D*). On the other hand, neuronal *hlh-30*-dependent differentially expressed genes (DEGs) in the *glp-1* background included GO terms different from *mml-1/mxl-2*, such as the biological processes involved in interspecies interactions between organisms, as well as stimulus responses and metabolism (*SI Appendix*, Fig. S5*E*). RNA-seq analysis consistently indicated that neuronal MML-1/MXL-2 regulated aging via downstream mechanisms distinct from neuronal HLH-30.

Neuronal MML-1/MXL-2 Transcriptionally Regulates *glt-5* Expression in Neurons to Modulate Autophagy and Longevity. To identify longevity-modulating factors downstream of neuronal MML-1/MXL-2, we set three criteria to select candidates: i) It is contained in the neuronal *mml-1/mxl-2* commonly regulated DEGs, ii) a putative human homolog exists, and iii) RNAi is contained in our *C. elegans* RNAi library. We suppressed 34 genes that met these criteria from eggs in neurons of *glp-1* mutants and measured survival rates at 25 d. After removing several clones whose knockdown from eggs caused developmental defects such as *mlt-7* and *his-6*, we decided to focus on *glt-5* for further analysis because only *glt-5* is specifically expressed in neurons among the candidates that abolished *glp-1* longevity (Fig. 3*A* and *SI Appendix*, Fig. S5*F*). GLT-5, an L-glutamate (Glu) transmembrane transporter, is predicted to prevent neurotoxic accumulation by excluding Glu from the synaptic cleft (49–52). Significantly, the transcription level of *glt-5* was increased by germline deficiency in a neuronal *mml-1/mxl-2*-dependent manner (Fig. 3*B*). Similarly, upregulation of *glt-5* expression in *glp-1* was impaired by depletion of *mml-1* or *mxl-2* (*SI Appendix*, Fig. S6*A*). Moreover, *mml-1* overexpression in neurons resulted in a more than twofold increase in *glt-5* transcription compared to WT animals (Fig. 3*C*). Using public scRNA-seq, We then found that *glt-5* as well as *mml-1/mxl-2* are expressed in neurons including PVR, ADL, and AVD (*SI Appendix*, Figs. S1 *G* and *H* and S6*B*). To gain further support for the MML-1/MXL-2-GLT-5 axis, we generated mNeonGreen knock-in strains and confirmed the neuronal expression of GLT-5::mNeonGreen (*SI Appendix*, Fig. S6 *D* and *E*). Consistent with the transcriptional change, the intensity of GLT-5::mNeonGreen in neurons was increased by germline deficiency in a neuronal *mml-1/mxl-2*-dependent manner (Fig. 3 *D* and *E*). These data further support our observation that neuronal *mml-1/mxl-2* positively regulates *glt-5* expression. Interestingly, *glt-5* transcriptional upregulation in *glp-1* mutants was not abolished by neuronal *hlh-30* knockdown, indicating that neuronal *glt-5* is a preferential target of MML-1/MXL-2 (*SI Appendix*, Fig. S6*C*).

We next tested whether neuronal GLT-5, like MML-1/MXL-2, regulates the autophagic activity in several tissues of germline-deficient animals. Similar to the knockdown of *mml-1/mxl-2*, we found that

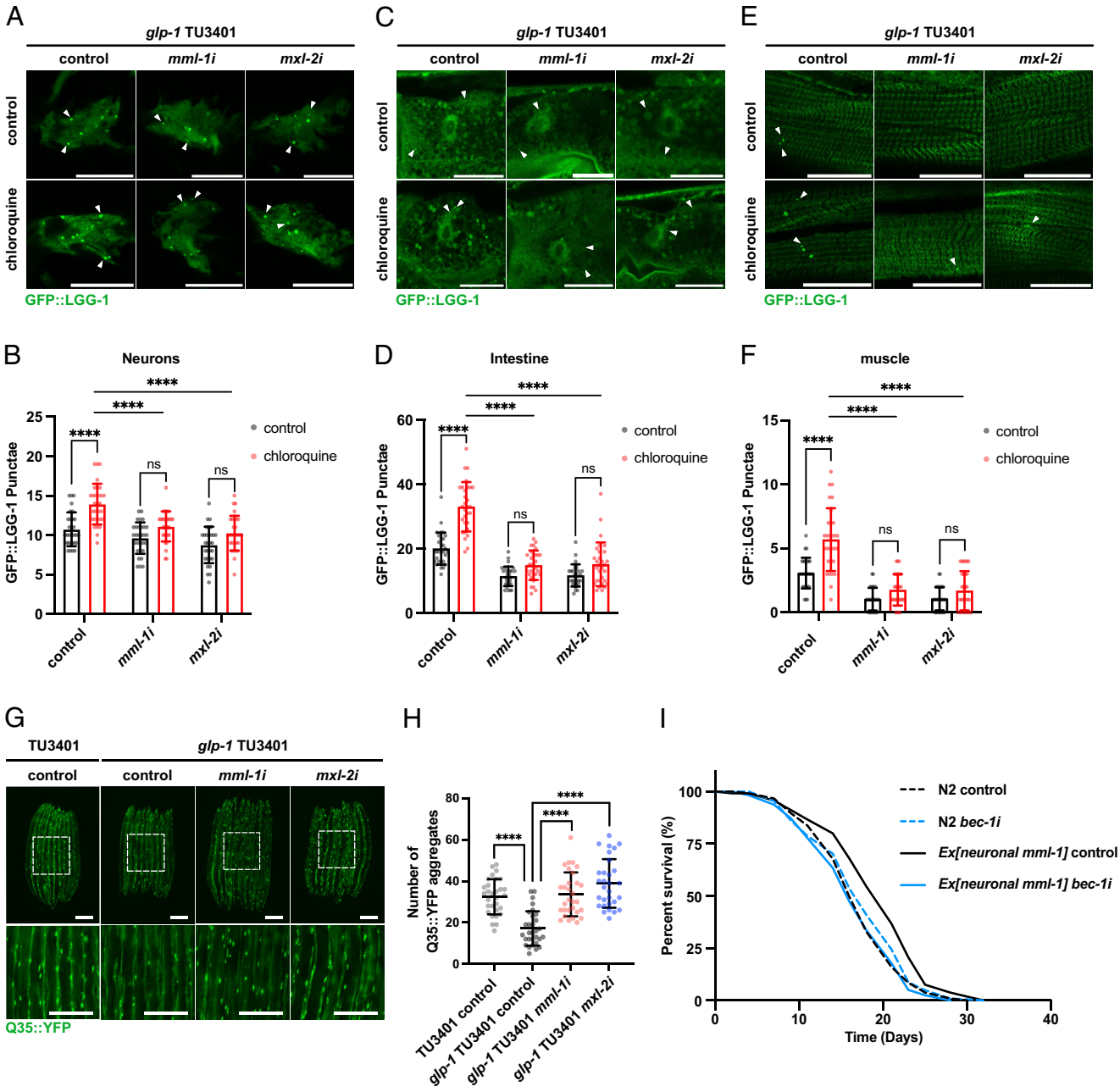

Fig. 2. Neuronal MML-1/MXL-2 regulates systemic autophagy to extend lifespan. (*A*) Autophagosomes in neurons were measured in neuronal *mml-1* or *mxl-2* knockdown *glp-1* worms expressing *rgef-1p::gfp::lgg-1*. Newly generated strains were obtained by crossing MAH242 and TU3401 with *glp-1(e2141)* mutation, and images were taken on adult day 1. Knockdown was conducted from egg onward. Worms were treated with 5 mM chloroquine or mock control. Arrowheads indicate GFP::LGG-1 puncta. (*B*) Quantification of GFP::LGG-1 puncta in neurons. Values represent means ± SD ($n = 30$). *P* values (ns (not significant) > 0.05, ****$P < 0.0001$) were determined by two-way ANOVA with Tukey's test. (*C*) Autophagosomes in the intestine were measured in neuronal *mml-1* or *mxl-2* knockdown *glp-1* worms expressing *lgg-1p::gfp::lgg-1*. Images were taken on adult day 1. Knockdown was conducted from egg onward. Worms were treated with 5 mM chloroquine or mock control. (*D*) Values represent mean ± SD ($n = 30$). *P* values (ns > 0.05, ****$P < 0.0001$) were determined by two-way ANOVA with Tukey's test. (*E*) Autophagosomes in muscle were measured in neuronal *mml-1* or *mxl-2* knockdown *glp-1* worms expressing *lgg-1p::gfp::lgg-1*. Images were taken on adult day 1. Knockdown was conducted from egg onward. Worms were treated with 5 mM chloroquine or mock control. (*F*) Values represent mean ± SD (n = 30). *P* values (ns > 0.05, ****$P < 0.0001$) were determined by two-way ANOVA with Tukey's test. (*G*) Images of body-wall muscle polyQ35::YFP with and without neuronal *mml-1i* or *mxl-2i* on adult day 4. *Mml-1* or *mxl-2* knockdown in neurons increased the age-dependent accumulation of polyQ aggregates in *glp-1(e2141)* mutants. (*H*) Quantification of the number of Q35::YFP aggregates in body-wall muscle. Values represent mean ± SD ($n = 30$). *P* values (****$P < 0.0001$) were determined by one-way ANOVA with Tukey's test. (*I*) The longevity of *rab-3p::mml-1::gfp* animals was abolished by *bec-1* RNAi. (Scale bars, 20 μm [*A*, *C*, and *E*], 200 μm [*G*].)

neuronal *glt-5* knockdown significantly reduced autophagy flux in several tissues including intestine and muscle (Fig. 3 *F-K*), indicating that neuronal *glt-5* downstream of *mml-1/mxl-2* regulates autophagy in the peripheral tissues. Consistently neuronal *glt-5i* decreased Q35::YFP aggregation in the muscle of *glp-1* mutants (Fig. 3 *L* and *M*). It is noted that autophagic flux in neurons was not completely inhibited by *glt-5* knockdown, in contrast to *mml-1/mxl-2* knockdown (Fig. 2 *A* and *B*), suggesting that *mml-1/mxl-2* regulates neuronal autophagy partly independently from *glt-5*.

Given that GLT-5 acts in neurons to regulate autophagy and longevity, we wondered if *glt-5* transcription is directly regulated by the MML-1/MXL-2 complex in neurons. MondoA/ChREBP, the human homolog of MML-1, recognizes the CACGTG E-box element subclass and activates transcription from it (53–56). We

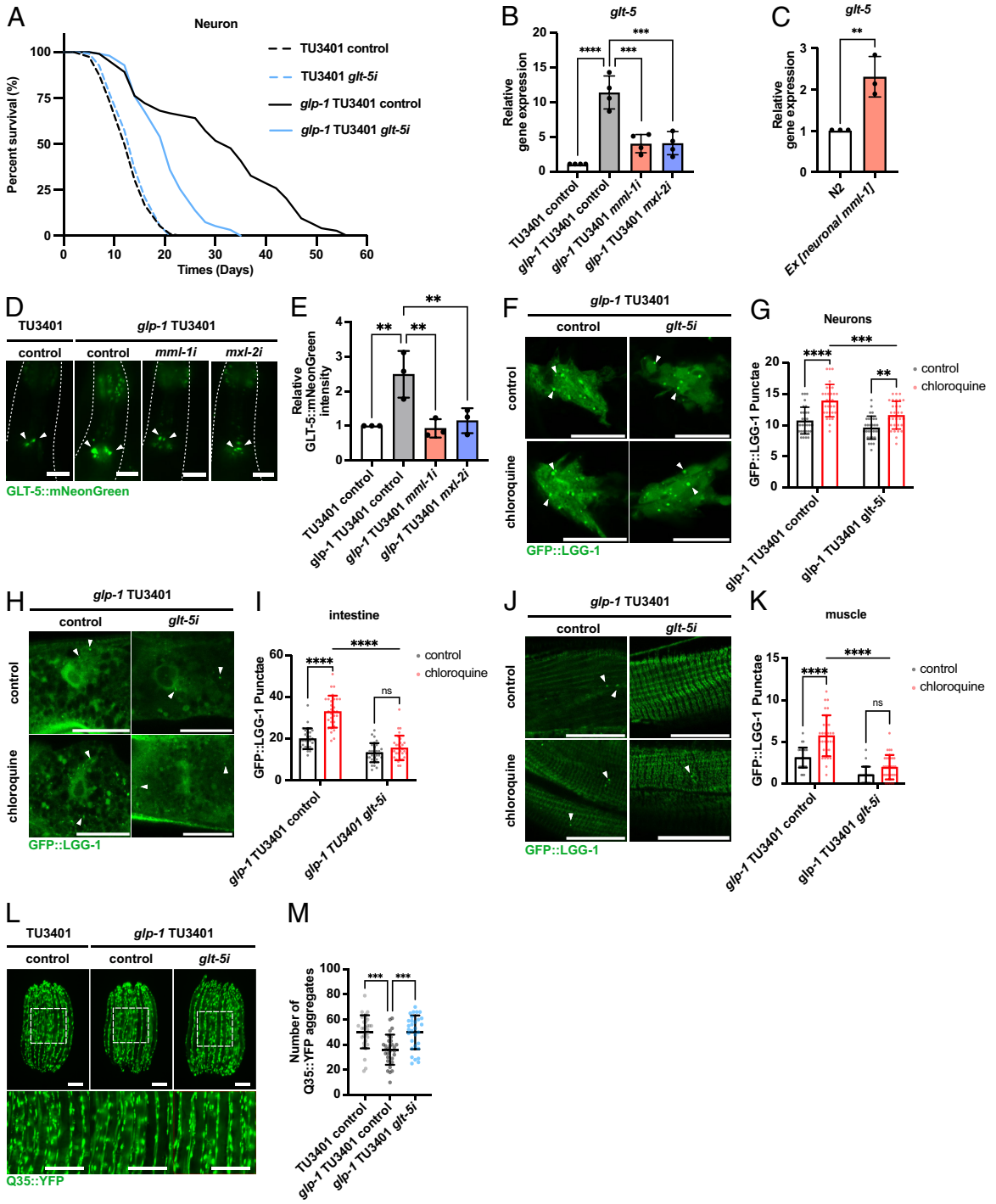

Fig. 3. Neuronal MML-1/MXL-2 regulates systemic aging by regulating glutamate transporter GLT-5. (*A*) Neuronal *glt-5* knockdown suppressed *glp-1 (e2141)* longevity. Knockdown was conducted from egg onward. (*B*) qRT-PCR analysis of *glt-5* expression on adult day 1. The mRNA levels of *glt-5* were increased by germline deficiency in a neuronal MML-1/MXL-2-dependent manner. Means ± SD from three independent experiments are depicted and were normalized to control TU3401 day 1 samples. *P* values (***$P < 0.001$ and ****$P < 0.0001$) were determined by one-way ANOVA with Tukey's test. (*C*) The transcription levels of *glt-5 were* increased in *rab-3p::mml-1::gfp*-expressing animals. Mean ± SD from three independent experiments are depicted and were normalized to control TU3401 day 1 samples. *P* values (**$P < 0.01$) were determined by one-way ANOVA with Tukey's test. (*D*) The representative fluorescent images of GLT-5::mNeonGreen knockin worms in neurons of TU3401 and *glp-1* TU3401 worms at day 1 young adult stage. Knockdown was conducted from egg onward. (*E*) Quantification of GLT-5::mNeonGreen in neurons. Values represent mean ± SD from three biological replicates (10 worms each). *P* values (**$P < 0.01$) were determined by one-way ANOVA with Tukey's test. (*F*) Autophagosomes in neurons were measured in neuronal *glt-5* knockdown *glp-1* worms expressing *rgef-1p::gfp::lgg-1*. Images were taken on adult day 1. Knockdown was conducted from eggs of parental generation. Worms were treated with 5 mM chloroquine or mock control. Arrowheads indicate GFP::LGG-1 puncta. (*G*) Quantification of GFP::LGG-1 puncta in neurons. Values represent mean ± SD ($n = 30$). *P* values (**$P < 0.01$, ***$P < 0.001$, and ****$P < 0.0001$) were determined by two-way ANOVA with Tukey's test. (*H*) Autophagosomes in the intestine were measured in neuronal *glt-5* knockdown *glp-1* worms. Images were taken on adult day 1. Knockdown was conducted from eggs of parental generation. Worms were treated with 5 mM chloroquine or mock control. (*I*) Values represent mean ± SD ($n = 30$). *P* values (ns > 0.05, ****$P < 0.0001$) were determined by two-way ANOVA with Tukey's test. (*J*) Autophagosomes in muscle were measured in neuronal *glt-5* knockdown *glp-1* worms. Images were taken on adult day 1. Knockdown was conducted from eggs of parental generation. Worms were treated with 5 mM chloroquine or mock control. (*K*) Values represent mean ± SD (n = 30). *P* values (ns > 0.05, ****$P < 0.0001$) were determined by two-way ANOVA with Tukey's test. (*L*) Images of body-wall muscle polyQ35::YFP with and without neuronal *glt-5* on adult day 4. Neuronal *glt-5* knockdown increased the age-dependent accumulation of polyQ aggregates in *glp-1(e2141)* mutants. (*M*) Quantification of the number of Q35::YFP aggregates in body-wall muscle. Values represent mean ± SD ($n = 30$). *P* values (***$P < 0.001$) were determined by one-way ANOVA with Tukey's test. (Scale bars, 20 μm [*D*, *F*, *H*, and *J*], 200 μm [*L*].)

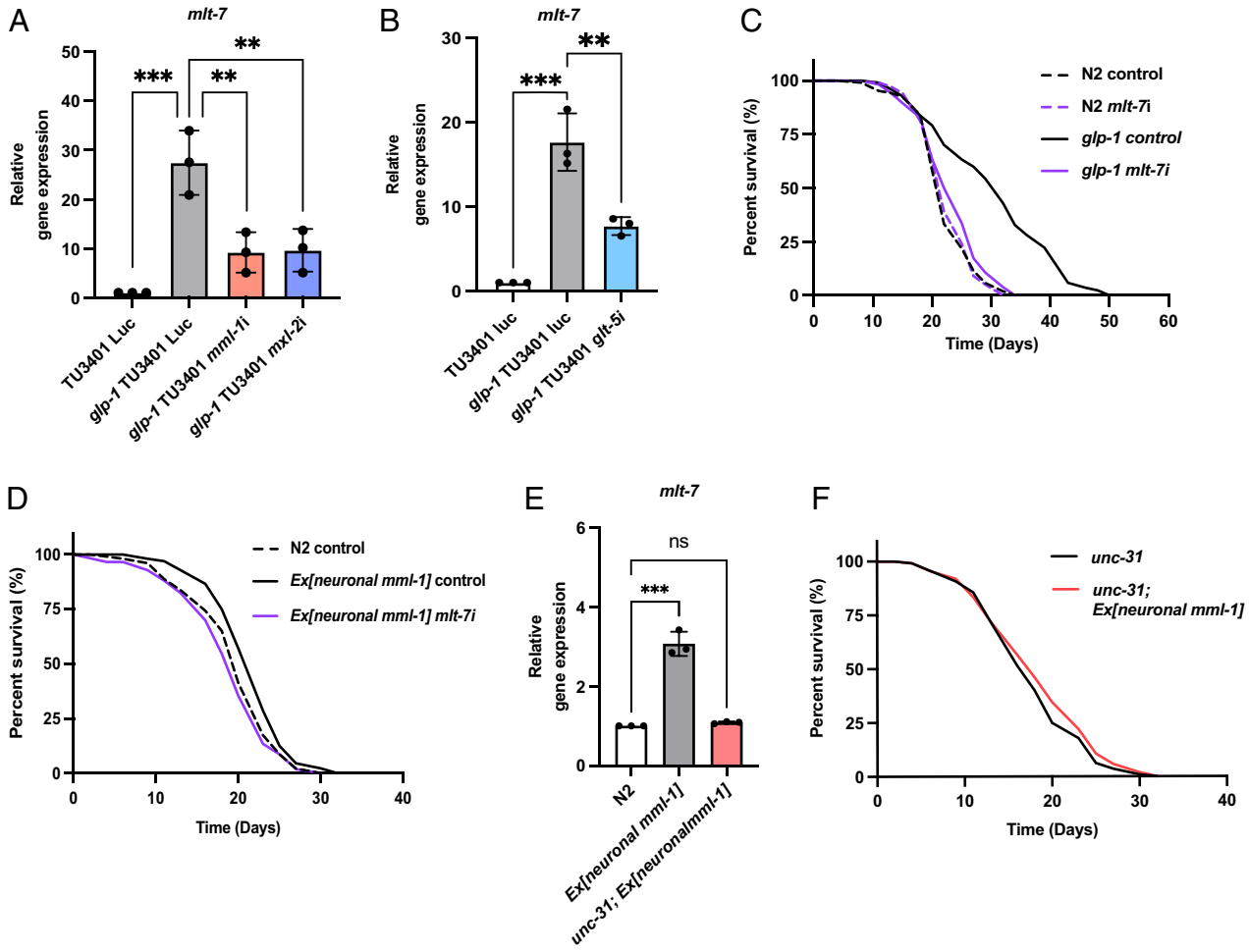

Fig. 4. MLT-7 contributes to lifespan extension downstream of neuronal MML-1/MXL-2-GLT-5 axis. (*A*) qRT-PCR analysis of *mlt-7* expression on adult day 1. The mRNA levels of *mlt-7* were increased by germline deficiency in a neuronal MML-1/MXL-2-dependent manner. Mean ± SD from three independent experiments are depicted and were normalized to control TU3401 day 11 samples. *P* values (***P* < 0.01 and ****P* < 0.001) were determined by one-way ANOVA with Tukey's test. (*B*) qRT-PCR analysis of *mlt-7* expression on adult day 1. Elevated transcription of *mlt-7* in *glp-1(e2141)* mutants was canceled by neuronal inhibition of *glt-5*. Means ± SD from three independent experiments are depicted and were normalized to control TU3401 day 1 samples. *P* values (***P* < 0.01 and ****P* < 0.001) were determined by one-way ANOVA with Tukey's test. (*C*) Inhibition of *mlt-7* by RNAi suppressed *glp-1(e2141)* longevity. Knockdown was conducted from L4 stage. The log-rank test was conducted for statistical analysis. (*D*) Longevity conferred by overexpression of *mml-1* in neurons was abolished by *mlt-7* knockdown. Knockdown was conducted from L4 stage. (*E*) qRT-PCR analysis of *mlt-7* expression on adult day 1. *Mlt-7* induction conferred by neuronal *mml-1* overexpression was abolished by *unc-31(e169)* mutation. Means ± SD from three independent experiments are depicted and were normalized to control N2 day 1 samples. *P* value (ns > 0.05, ****P* < 0.001) was determined by one-way ANOVA with Tukey's test. (*F*) Longevity conferred by overexpression of *mml-1* in neurons was abolished by *unc-31(e169)* mutation.

found that a CACGTG E-box sequence that can bind to the MML-1/MXL-2 complex was conserved at about 550 base pairs upstream of the *glt-5* cording region (*SI Appendix*, Fig. S6*F*). Moreover, chromatin immunoprecipitation sequencing (ChIP-seq) data performed using modENCODE and available in the public domain shows that MML-1::GFP binds to the promoters for *glt-5* (*SI Appendix*, Fig. S6*G*) (57), further supporting the direct transcriptional regulation of *glt-5* by MML-1/MXL-2.

MLT-7 Acts in Peripheral Tissues Downstream of Neuronal MML-1/MXL-2 to Regulate *glp-1* Longevity. Since suppression of neuronal *mml-1/mxl-2* accelerates aging in peripheral tissues, we hypothesized that neuronal MML-1/MXL-2 regulates the expression and/or activity of specific lifespan-regulating genes in distal tissues. To further elucidate the intertissue-signaling that regulates longevity via the neuronal MML-1/MXL-2-GLT-5 axis, we explored genes that are down-regulated in *glp-1* mutants, with neuronal *mml-1*, *mxl-2*, or *glt-5i* among the neuronal *mml-1/mxl-2*-dependent DEGs. Through qRT-PCR-based screening, we identified that the expression of *mlt-7,* a heme peroxidase, was increased by germline deficiency in a manner dependent on the expression of neuronal *mml-1/mxl-2* and *glt-5* (Fig. 4 *A* and *B* and *SI Appendix*, Fig. S7 *A* and *B*). The fact that neuronal *hlh-30* was not necessary for transcriptional activation of *mlt-7* further substantiates that neuronal MML-1/MXL-2-mediated longevity is independent of neuronal HLH-30 (*SI Appendix*, Fig. S7*C*). We then examined whether MLT-7 was responsible for the longevity of germlineless animals and found that *glp-1* longevity was completely abolished by adult only *mlt-7* RNAi in WT and *glp-1* worms but not in neuronal knockdown strains (Fig. 4*C* and *SI Appendix*, Fig. S7*E*). Of note, adult only knockdown of *mlt-7* could bypass the requirement of this gene during development. Crucially, *mlt-7* knockdown eliminated the beneficial effects of neuronal *mml-1* on longevity (Fig. 4*D*). Considering the fact that neurons of WT worms are resistant to RNAi, these results suggest that neuronal MML-1-mediated longevity relies on nonneuronal MLT-7 function, implying the presence of neuron-to-peripheral communication.

To understand this neuron-to-peripheral communication, we examined whether *mlt-7* induction by neuronal overexpression of *mml-1* depends on UNC-31, which promotes neuropeptide

release from dense core vesicles or UNC-13, which mediates neurotransmitter release from synaptic vesicles (58, 59). We found that *unc-31* mutation abolished the induction of *mlt-7* on neuronal *mml-1* OE worms (Fig. 4*E*), while *unc-13* depletion rather slightly increased *mlt-7* expression (*SI Appendix*, Fig. S7*F*). Consistently, *unc-31*, but not *unc-13* was required for the longevity of neuronal *mml-1* OE worms (Fig. 4*F* and *SI Appendix*, Fig. S7*G*). These results indicate that neuropeptides are involved in neuronal *mml-1*-dependent *mlt-7* induction and longevity.

MLT-7 forms a complex with the dual oxidase (DUOX) protein BLI-3 at the plasma membrane and regulates H_2O_2 concentrations by converting BLI-3-generated H_2O_2 into H_2O, thus contributing to pathogen defense, oxidative stress resistance, extracellular matrix integrity, and aging (60–65). These findings led us to consider that the DUOX system, not just MLT-7 alone, is essential for *glp-1* longevity. In testing this hypothesis, we found that both RNAi and knockout of *bli-3* fully abrogated the lifespan extension in *glp-1* mutants (*SI Appendix*, Fig. S7 *H* and *I*). Interestingly, the expression of *bli-3, tsp-15*, and *doxa-1*, all of which are associated with DUOX systems, was up-regulated in germlineless animals, even though their upregulation was independent of neuronal *mml-1/mxl-2* (*SI Appendix*, Fig. S7 *J–L*). In short, *glp-1* longevity requires BLI-3 as well as MLT-7, but the upstream signaling regulating transcription is likely to differ between the two proteins.

Intestinal MLT-7 Promotes Longevity by Suppressing Age-Associated Reactive Oxygen Species (ROS) Accumulation. To understand how peripheral MLT-7 modulates aging, we first verified whether MLT-7 influenced autophagy in germlineless animals. Systemic RNAi of *mlt-7* did not affect the number of GFP::LGG-1 puncta in the pharynx, intestine, or muscle of *glp-1* mutants (*SI Appendix*, Fig. S8 *A–D*). In addition, suppression of autophagic activity by *bec-1* or *atg-9* RNAi did not affect *mlt-7* mRNA levels (*SI Appendix*, Fig. S8*E*), indicating that MLT-7 and autophagy regulate aging in parallel.

According to Harman's free-radical theory of aging, lifespan is decreased by the accumulation of molecular damage by ROS generated as metabolic byproducts (66). Contrary to this theory, accumulated evidence shows that ROS is not just a metabolic byproduct, but a rather beneficial signaling molecule (67–69). Although this hypothesis is still under debate, it is now considered that ROS are molecules that have opposing effects on the survival of organisms. In *C. elegans*, it has been reported that adequate levels of ROS are beneficial (64, 70, 71), whereas excessive accumulation is detrimental (72–74). Since MLT-7 can reduce ROS accumulation, we next hypothesized that MLT-7 activation leads to lifespan extension by preventing age-related accumulation of detrimental ROS. To analyze the effect of MLT-7 on redox homeostasis, we asked if *mlt-7* inhibition increases age-dependent ROS accumulation in *glp-1* mutants. Concentrations of dihydroethidium (DHE), a fluorogenic dye useful to detect ROS levels, were lower in *glp-1* mutants on adult day 8 compared to WT (Fig. 5 *A* and *B*). However, *mlt-7* RNAi drastically increased age-related ROS accumulation in *glp-1* mutants. To determine whether the reduced lifespan of *glp-1* mutants by *mlt-7* RNAi is caused by increased age-related ROS accumulation, we treated *glp-1* worms with the ROS scavenger N-acetylcysteine (NAC) and then measured lifespans. Indeed, treatment with 2 mM NAC partially restored the reduced lifespan of *glp-1* mutants caused by *mlt-7* knockdown (Fig. 5*C*), without affecting the lifespan of *glp-1* control worms (*SI Appendix*, Fig. S9*A*) (70). These data support our theory that a reduction in age-related detrimental ROS by MLT-7 slows aging in germlineless animals. Furthermore, the reduced lifespan of the *glp-1* mutants by suppression of neuronal *mml-1* was also rescued by NAC administration (*SI Appendix*, Fig. S9*B*), highlighting the lifespan-regulating role of the signaling cascade from neuronal MML-1/MXL-2 to peripheral MLT-7.

We then tried to identify the critical tissues in which MLT-7 acts to contribute to lifespan extension. As systemic RNAi of *mlt-7* increased ROS accumulation in the intestine (Fig. 5 *A* and *B*), we asked whether intestine-specific *mlt-7* knockdown is sufficient to cancel *glp-1* longevity. Suppression of *mlt-7* in the intestine significantly abolished *glp-1* longevity (Fig. 5*D*). Moreover, the negative effect of intestine-specific *mlt-7* inhibition was ameliorated by NAC administration (Fig. 5*E*). Taken together, these results indicate that to extend lifespan, it is important to prevent intestinal ROS accumulation through MLT-7 activation.

Discussion

The MML-1/MXL-2 complex is known to be required for multiple longevity pathways, but the underlying mechanism was not well understood. Our findings provide critical insights into the tissue specificity of MML-1/MXL-2. Although germline deficiency induces nuclear translocation of MML-1/MXL-2 throughout the body, MML-1/MXL-2 is required in neurons for the regulation of systemic aging. Importantly, neuronal MML-1/MXL-2 modulates autophagic and peroxidase MLT-7 activities in peripheral tissues via increased transcription of *glt-5* in neurons, which ultimately prolongs lifespan (*SI Appendix*, Fig. S10).

A growing number of studies have indicated that nervous system plays a central role in controlling health and aging in a variety of organisms, including worms, flies, and mammals (75). Our finding that neuronal MML-1/MXL-2 regulates systemic autophagy and aging supports this idea. Surprisingly, even neuronal overexpression of *mml-1* alone had a significant antiaging effect, suggesting that neuronal MML-1 could be an important potential target for regulating organismal health and aging. We also found that neuronal suppression of *mml-1/mxl-2* and *glt-5* influences autophagic activity in peripheral tissues in addition to neurons, suggesting that neuronal MML-1/MXL-2-GLT-5 axis regulates autophagy both in cell autonomous and cell nonautonomous manner. Actually, some *atgs* transcripts tended to be reduced by neuronal knockdown of *mml-1/mxl-2* (*SI Appendix*, Fig. S4 and Dataset S1). Thus, it is possible that neuronal *mml-1/ mxl-2* regulates *atgs* transcription in a cell-autonomous manner, but the changes are too small to be captured by a whole-organismal-level analysis. It is important to note that neuronal knockdown of *glt-5* did not completely abrogate autophagy flux, while knockdown of *mml-1/mxl-2* did, suggesting that *mml-1/mxl-2* regulates autophagy in neurons partly independent from *glt-5*.

Although previous studies have suggested that MML-1 and HLH-30 are mutually regulated and share target genes at an organismal level (16), our data intriguingly suggest that they have largely different targets in neurons. The downstream mechanism of neuronal HLH-30 in lifespan extension remains elusive, but we confirmed that it was not involved in the transcriptional regulation of *glt-5* and *mlt-7*. In addition, it is implied that the temporal requirements of neuronal MML-1 and HLH-30 may be different in order to extend lifespan of *glp-1* mutants, which provides further evidence that these factors can act independently, especially in neurons. While MML-1 overexpression sufficed to extend lifespan, HLH-30 overexpression did not. Interestingly, recent study shows that neuronal HLH-30 overexpression sufficed to improve heat stress resistance, suggesting that neuronal HLH-30 has a beneficial role only under the stressed condition. Importantly, neuronal HLH-30 mediates heat tolerance via W06A11.1 (76), however, neuronal suppression of *hlh-30* did not affect W06A11.1

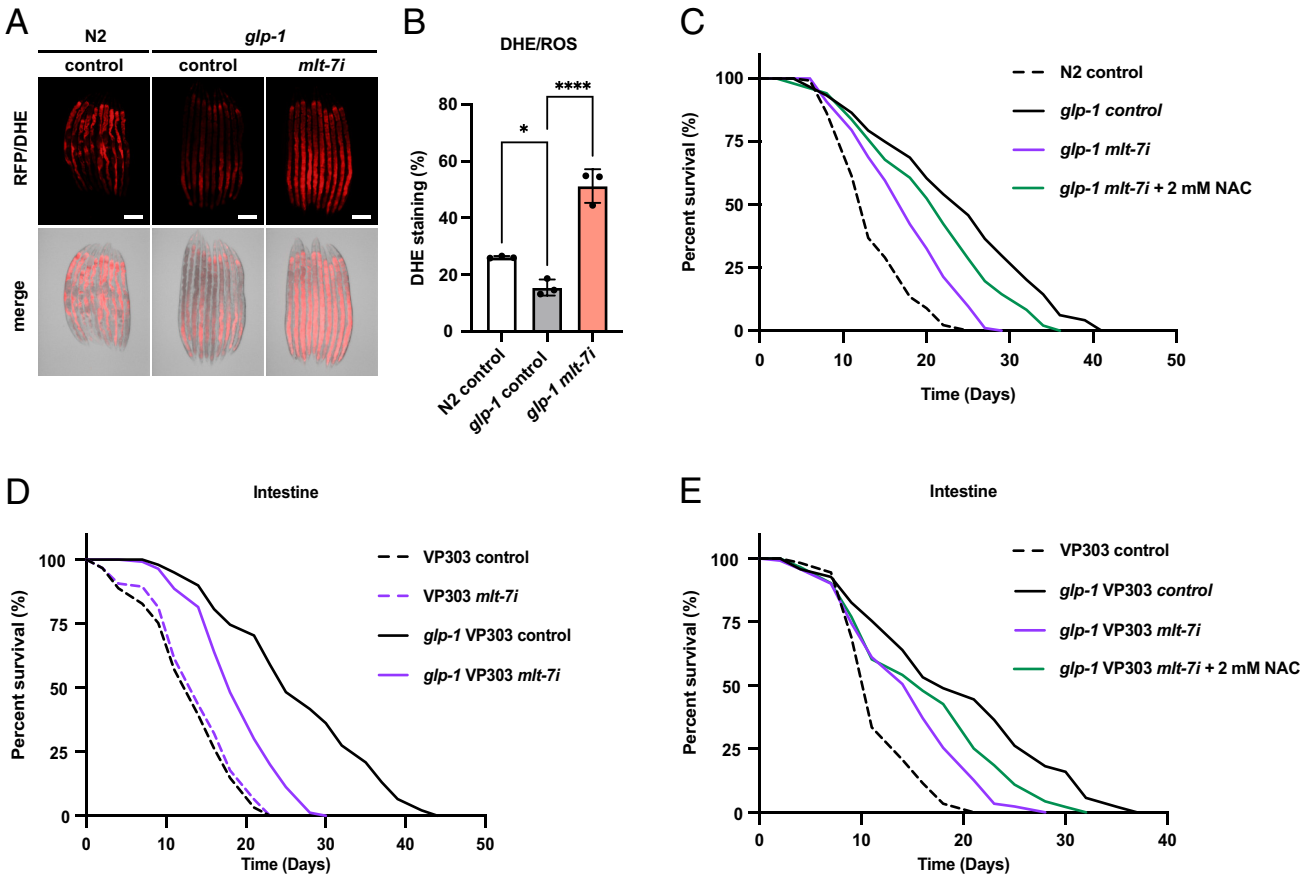

Fig. 5. MLT-7 regulates aging by eliminating detrimental ROS. (*A*) *mlt-7* knockdown increased age-dependent ROS accumulation in *glp-1(e2141)* mutants. The levels of ROS accumulation were detected by DHE staining. (*B*) Quantification of ROS accumulation in worms. The fluorescence intensity of worms at adult day 8 was quantified using ImageJ (Wayne Rasband) by determining the average intensity. Mean ± SD from three independent experiments are depicted. *P* values (**P* < 0.05 and *****P* < 0.0001) were determined by one-way ANOVA with Tukey's test. (*C*) Systemic RNAi of *mlt-7* abolished *glp-1* longevity. The lifespan of *glp-1(e2141)* mutants, which was reduced by *mlt-7i,* was rescued by administration of 2 mM NAC. Knockdown was conducted from L4 stage. (*D*) Intestinal knockdown of *mlt-7* was sufficient to reduce *glp-1(e2141)* longevity. VP303 (a strain sensitive to intestine-specific RNAi) was used and knockdown was conducted in L4 worms. (*E*) The lifespan of *glp-1(e2141)* mutants, which was reduced by intestinal *mlt-7i,* was rescued by administration of 2 mM NAC. Knockdown was conducted from L4 stage. (Scale bars, 200 μm [*A*].)

transcript in our RNAseq data (Dataset S1), suggesting that presence of context-specific HLH-30 regulatory mechanism as shown in the previous work (77).

Glutamate is a major excitatory neurotransmitter that regulates functions such as memory and learning. Excessive glutamate concentrations in the synaptic cleft trigger glutamate excitotoxicity and damage neuronal cells (78, 79). Therefore, these concentrations must be tightly controlled, and glutamate transporters play a role in this process. One highlight of our study is that cell nonautonomous activation of autophagic and peroxidase activity by neuronal MML-1/MXL-2 was mediated by neuronal GLT-5. These observations raise the question of how elevated expression of glutamate transporters in neurons regulates systemic aging. Important insights into this issue were provided by previous observations showing that excitotoxicity, which contributes to neuronal injury and death in neurodegenerative diseases, is associated with EAAT2, the mouse homolog of GLT-5. Loss of EAAT2 function may be associated with chronic neurodegenerative diseases such as Alzheimer's disease and amyotrophic lateral sclerosis (80–82). Moreover, several lines of evidence indicate that approaches to increase EAAT2 activity have the potential to suppress excitotoxicity and prevent neurodegenerative diseases (83, 84). Based on these reports, it is plausible that neuronal MML-1/MXL-2 exerts a neuroprotective effect against glutamate-induced cytotoxicity by up-regulating GLT-5 in neurons, which results in the stable production and/or release of specific signal molecules that activate autophagy and MLT-7 in peripheral tissues. Our epistatic analysis revealed that at least the release of neuropeptide mediates longevity and *mlt-7* expression by neuronal *mml-1* overexpression. Further detailed analysis is required to examine if the neuropeptides function downstream of GLT-5 and if so, what exactly kinds of neuropeptides are involved in these processes. It could be also possible that lifespan is extended by enhanced glutamate metabolism and recycling via GLT-5 activation rather than protection from glutamate neurotoxicity. Glutamate transported into astrocytes by EAAT2 is recycled in a process known as the glutamate–glutamine cycle. This process is closely associated with neuronal energy metabolism and is essential for maintaining glutamatergic neurotransmission (85, 86). In addition, glutamate in astrocytes can be converted to α-ketoglutarate by glutamate dehydrogenase, which then confluences with the tricarboxylic acid cycle. In any case, understanding how GLT-5 acts in neurons to regulate systemic aging is an important future goal.

Finally, this work reveals the importance of eliminating age-associated intestinal ROS by peroxidase MLT-7 to extend lifespan. Contrary to this finding, however, recent studies have suggested that ROS may provide beneficial effects on lifespan. For example, in a subpopulation of synchronized worms, those with higher ROS levels during early development tended to have higher stress tolerance and longer lifespan (71). Moreover, compared to

WT animals, those that are germline deficient have higher ROS levels detected by DHE at adult day 1 (70). This high level of ROS at young ages activates the transcription factor DVE-1-dependent mitochondrial UPR and extends lifespan. Importantly, when *mlt-7* was suppressed in *glp-1* mutants, we found no increase in ROS accumulation at adult day 4, but a significant increase was seen at adult day 8. This implies that MLT-7 has little effect on ROS in early life and is mainly responsible for reducing age-associated detrimental ROS. Several recent studies (70, 71), in addition to our own, have manifested two opposite effects of ROS on longevity: moderate exposure to ROS in young animals, especially during development, induces hormesis and has a positive effect on lifespan, while excessive ROS accumulation in older animals disrupts cellular homeostasis and has a negative effect on lifespan.

Material and Methods

Worm Growth Conditions and Strains. Nematodes were maintained at 20 °C using standard techniques on NGM plates with *Escherichia coli* strain OP50 unless otherwise noted (87). Strains with the temperature-sensitive *glp-1(e2141)* mutation were maintained at 15 °C and grown at 25 °C to induce the germline-deficient phenotype. The list of all strains used in this study is presented in *SI Appendix*, Table S1.

Plasmid Construction and Transgenesis. For *rab-3p::mml-1::GFP* and *rab-3p::hlh-30::GFP* translational fusion constructs, the *rab-3* 3-kb endogenous promoter and the *mml-1/hlh-30* endogenous cording sequence were cloned into a pDC4 vector containing the EGFP tag. Microinjection of the construct was carried out with the coinjection marker *lin-44p::RFP* to generate *rab-3p::mml-1::GFP* and *rab-3p::hlh-30::GFP* transgenic worms. The *glt-5::mNeonGreen and hlh-30::mNeonGreen* knock-in worms was generated by SunyBiotech.

RNAi. RNAi was carried out by feeding worms with HT115 (DE3) bacteria transfected with the L4440 vector, which induces the expression of dsRNA against the targeted gene. Synchronized worms were cultured on the RNAi plates containing isopropyl β-D-thiogalactopyranoside and ampicillin. RNAi clones were obtained from the Ahringer *C. elegans* RNAi feeding library. RNAi against Luciferase (L4440::Luc) was used as nontargeting control.

Lifespan Analysis. Synchronous populations were obtained from 6 h egg lays on NGM plates with OP50 or RNAi plates. On day 1 of adulthood, 120 nematodes were transferred to six plates containing FUdR and grown at 20 °C. On day 5 of adulthood, they were placed on FUdR-free plates and then periodically transferred to new plates. Survivorship was assessed every 2 or 3 d. In the case of the *glp-1(e2141)* background, synchronized eggs were cultured at 25 °C for 2 d and then transferred to 20 °C from the day 1 adult stage. Whether or not animals were alive or dead was determined by the presence or absence, respectively, of a response to stimulation with a platinum wire. Worms were censored if they demonstrated internal hatching or bursting vulva, or if they crawled off the plates. In order to examine the temporal requirements of neuronal *mml-1* and *hlh-30* in longevity, synchronized worms were cultured on RNAi plates against Luciferase and then transferred to the target RNAi plates from a specific day. For statistics, we used an in-house Microsoft Excel (Microsoft) data sheet that could run a log-rank test. The experiments were repeated two or three times. All lifespan experiments in worms, including repeats, are presented in *SI Appendix*, Table S2.

Microscopy and Quantification. For quantification of HLH-30::mNeonGreen, HLH-30::GFP, and GLT-5::mNeonGreen, animals were anesthetized in 0.5% 1-Phenoxy-2-propanol or 0.1% sodium azide, and pictures were taken at the same exposure time using an FV3000 confocal microscope (Olympus) or SZX16 stereomicroscope (Olympus). Fluorescence intensity in nerve-ring neurons (HLH-30::mNeonGreen and GLT-5::mNeonGreen), the head region (HLH-30::GFP), the intestine (HLH-30::mNeonGreen), hypodermis (HLH-30::mNeonGreen), or muscle (HLH-30::mNeonGreen) was measured and quantified using Image J (Wayne Rasband). For the nuclear localization assay of MML-1::GFP, animals were anesthetized in 0.1% sodium azide at day 1 of adulthood and the numbers of animals carrying nuclear MML-1::GFP in nerve-ring neurons were quantified. Ten worms were scored in each experiment, and all experiments were repeated at least three times for all microscopy experiments.

RNA Extraction and qRT-PCR. *C. elegans* samples were harvested in QIAZOL (QIAGEN) at various time points. A total of 200 to 300 worms were collected per condition, and total RNA was extracted using the RNeasy® mini kit (QIAGEN). cDNA was generated using iScript (Bio-Rad). Power SYBR Green (Applied Biosystems) was used to perform qRT-PCR on a QuantStudio 7 Flex Real-Time PCR System (Thermo Fisher Scientific). Three or four technical replicates were conducted for each experiment. *ama-1* was used as internal control. Sequences of primers for qRT-PCR are shown in *SI Appendix*, Table S3.

Locomotion Assay. Locomotion assay was conducted as previously described (88). Worms were transferred to 6 cm NGM plates 30 min before measurement. Plates with worms from a given experimental group were placed in one of four regions, and multiple experimental groups were evaluated at the same time. An adapted version of the MWT (37) was used to record locomotion on agar plates for 10 min under dark-field lighting conditions using a Toshiba-Teli Ultra High Resolution 12 megapixel CMOS sensor camera-link camera (CSC12M25BMP19-01B), a lens (RICOH, FL-YFL3528), an adaptor (Toshiba-Teli, FTAR-2), and a ring LED light (CCS, LDR-206SW2-LA1). Recorded data were analyzed using Choreography (part of the MWT software), and organized and summarized using custom-written scripts. The initial 8 min of each recording were disregarded to allow tracker recognition to stabilize. Animal tracks were collected as time series of centroid positions for each frame in the final 2 min. The following Choreography filters were applied to prevent image artifacts: –shadowless and –t 10. The speed of an individual worm was calculated as the total distance between consecutive centroids, divided by the duration of the track. The mean and SEM, weighted by the length of an animal's track, were used to summarize the experimental groups. The experiments were repeated three times.

Lipofuscin Accumulation Assay. Nematodes were anesthetized in 0.1% sodium azide after washing with M9 buffer. Worms were then aligned on foodless NGM plates, and images were acquired using an SZX16 stereomicroscope (Olympus) with a GFP filter set. The autofluorescence intensity was measured using ImageJ (Wayne Rasband) software. The experiments were repeated three times.

Intestinal Barrier Function Assay. The intestinal barrier function of *C. elegans* was assessed by counting the ratio of dye leakage from the intestine as previously described (39). Briefly, more than 50 animals were collected with M9 from plates on particular days and suspended for 3 h in liquid cultures of overnight-grown OP50 bacteria mixed with FD&C blue (5% w/v in water). Worms were then transferred to precooled plates and analyzed for the presence or absence of blue food dye in the body cavity using an SZX16 stereomicroscope (Olympus). For quantification of the Smurf phenotype, we counted as leaked worms only those with a blue signal over the entire body. The experiments were repeated three times, each with approximately 40 animals per experimental group.

Heat-Stress Resistance Assay. Synchronized worms were grown at 25 °C until adult day 1. Twenty animals were transferred to a new plate and subjected to heat stress (35 °C) in an incubator for 8 h, and surviving animals were then counted. The experiments were repeated three times.

Quantification of Autophagy Flux. GFP::LGG-1-expressing worms at day 1 adulthood were transferred onto RNAi plates with or without 5 mM chloroquine and incubated for 24 h to inhibit autophagic flux by decreasing autophagosome-lysosome fusion in each tissue. Worms were anesthetized with 0.1% sodium azide and mounted on a 1% agarose pad. Images were acquired using an FV3000 confocal microscope (Olympus). For each experiment, the Z position adopted was based on whether or not the following could be clearly observed: nucleus (for intestine), and striation (for muscle). GFP-positive puncta in the neuronal, intestinal, or muscular regions were counted and quantified. Images of 10 worms in each condition were captured and the experiments were repeated three times.

Quantification of polyQ Aggregates. Animals were raised as described above for the lifespan assay until day 4 of the adult stage. Ten animals were anesthetized with 0.1% sodium azide and placed on foodless plates, and images were acquired using an SZX16 stereomicroscope (Olympus). The number of Q35::YFP aggregates was counted using ImageJ (Wayne Rasband). Aggregates were defined as

discrete structures with boundaries distinguishable from surrounding fluorescence on all sides. The experiments were repeated three times.

RNA-Seq. RNA-seq was carried out at the Center of Medical Innovation and Translational Research of Osaka University. The TruSeq Stranded mRNA Library Prep Kit (Illumina, 20020594) was used to prepare RNA-seq libraries, and capillary electrophoresis was used to assess the quality and quantity of samples. Libraries were analyzed by qPCR, processed for immobilization in flow cells using cBot (Illumina), and then conducted sequence-by-synthesis with a NovaSeq 6000 S4 system on a NovaSeq 6000 at Macrogen-Japan. GO annotation and enrichment analysis was performed using DAVID.

ROS Measurement. ROS accumulation in *C. elegans* was detected using the ROS-sensitive dye DHE (Thermo Fisher Scientific, D11347). Synchronized worms on NGM plates were washed with M9 buffer and then incubated in M9 buffer containing 3 μM DHE for 30 min at room temperature. After incubation, worms were washed with M9 again and lined up on a pre-cooled plate. ROS signals were detected using an SZX16 stereomicroscope (Olympus). The experiments were repeated three times.

Western Blotting. Animals were lysed in lysis buffer (50 mM Tris/HCl [pH 7.4], 150 mM NaCl, 1 mM EDTA, 0.1% NP-40) using a homogenizer. After centrifugation, the supernatants were heated at 95 °C for 7 min. The lysates were separated by SDS-PAGE, and transferred to PVDF membranes that were then blocked and incubated with specific primary antibodies. Primary antibodies and dilutions were as follows: p38 MAPK (Cell Signaling Technology, #9212, 1:2,000), Phospho-p38 MAPK (Cell Signaling Technology, #9211, 1:2,000), and α-Tubulin (Sigma-Aldrich, A11126, 1:10,000). The intensities were quantified using ImageLab (Bio-Rad).

Statistical Analysis. The experimental results were performed using GraphPad Prism 9 software (GraphPad Software) or Microsoft Excel (Microsoft). Statistical analysis was performed using either the *t* test or one-way ANOVA with Tukey's test. Data are presented as vertical scatter plots with mean ± SD.

Data, Materials, and Software Availability. All study data are included in the article and/or supporting information. RNA-Seq data are deposited at the Gene Expression Omnibus (GSE234429, and GSE234430) (89, 90).

ACKNOWLEDGMENTS. We thank Prof. Kimura (Nagoya City University) for providing the *rab-3* promoter. We thank Osaka University Medical Innovation and Translational Research Center for assistance and access to experimental equipment and technical support. We also thank the *Caenorhabditis* Genetics Center at the University of Minnesota. *C. elegans* RNAi clones for *mlt-7* were kindly provided by Prof. Nishiwaki (Kwansei Gakuin University). T.Y. is supported by Japan Society for the Promotion of Science (JSPS) KAKENHI (22H04982), Japan Agency for Medical Research and Development (AMED) (grant no. JP22gm1410014), and the Takeda Science Foundation. S.N. is supported by AMED-PRIME (20gm6110003h0004), MEXT KAKENHI, a Grant-in-Aid for Transformative Research Areas B (21H05145), JSPS KAKENHI (21H02428 and 19K22429), the Astellas Foundation for Research on Metabolic Disorders, the Mochida Memorial Foundation for Medical and Pharmaceutical Research, the Mitsubishi Foundation, Research Grants in the Natural Sciences, and the NOVARTIS Foundation (Japan) for the Promotion of Science. T.S. is supported by JSPS KAKENHI (22J13562).

Author affiliations: [a]Laboratory of Intracellular Membrane Dynamics, Graduate School of Frontier Biosciences, Osaka University, Osaka 565-0871, Japan; [b]Department of Neurology, Graduate School of Medicine, Osaka University, Osaka 565-0871, Japan; [c]Cell Biology Center, Institute of Innovative Research, Tokyo Institute of Technology, Yokohama 226-8503, Japan; [d]Graduate School of Life Science and Technology, Tokyo Institute of Technology, Yokohama 226-8503, Japan; [e]Department of Cellular Physiology, Graduate School of Medical and Dental Sciences, Niigata University, Niigata 951-8510, Japan; [f]Department of Life Science, Rikkyo University, Tokyo 171-8501, Japan; [g]Department of Molecular Genetics of Ageing, Max Planck Institute for Biology of Ageing, Cologne 50931, Germany; [h]Cologne Excellence Cluster on Cellular Stress Responses in Aging Associated Diseases, University of Cologne, Cologne 50931, Germany; [i]Department of Genetics, Graduate School of Medicine, Osaka University, Osaka 565-0871, Japan; [j]Integrated Frontier Research for Medical Science Division, Institute for Open and Transdisciplinary Research Initiatives, Osaka University, Osaka 565-0871, Japan; and [k]Institute for Advanced Co-Creation Studies, Osaka University, Osaka 565-0871, Japan

1. C. J. Kenyon, The genetics of ageing. *Nature* **464**, 504–512 (2010).
2. L. R. Lapierre, M. Hansen, Lessons from *C. elegans*: Signaling pathways for longevity. *Trends Endocrinol. Metab.* **23**, 637–644 (2012).
3. C. Kenyon *et al.*, A *C. elegans* mutant that lives twice as long as wild type. *Nature* **366**, 461–464 (1993).
4. J. M. Tullet *et al.*, Direct inhibition of the longevity-promoting factor SKN-1 by insulin-like signaling in *C. elegans*. *Cell* **132**, 1025–1038 (2008).
5. A. L. Hsu, C. T. Murphy, C. Kenyon, Regulation of aging and age-related disease by DAF-16 and heat-shock factor. *Science* **300**, 1142–1145 (2003).
6. B. N. Heestand *et al.*, Dietary restriction induced longevity is mediated by nuclear receptor NHR-62 in *Caenorhabditis elegans*. *PLoS Genet.* **9**, e1003651 (2013).
7. T. T. Ching *et al.*, drr-2 Encodes an eIF4H that acts downstream of TOR in diet-restriction-induced longevity of *C. elegans*. *Aging Cell* **9**, 545–557 (2010).
8. S. K. Park, C. D. Link, T. E. Johnson, Life-span extension by dietary restriction is mediated by NLP-7 signaling and coelomocyte endocytosis in *C. elegans*. *FASEB J.* **24**, 383–392 (2010).
9. S. H. Panowski *et al.*, PHA-4/Foxa mediates diet-restriction-induced longevity of *C. elegans*. *Nature* **447**, 550–555 (2007).
10. N. Libina, J. R. Berman, C. Kenyon, Tissue-specific activities of *C. elegans* DAF-16 in the regulation of lifespan. *Cell* **115**, 489–502 (2003).
11. M. Uno *et al.*, Neuronal DAF-16-to-intestinal DAF-16 communication underlies organismal lifespan extension in *C. elegans*. *iScience* **24**, 102706 (2021).
12. R. C. Taylor, A. Dillin, XBP-1 is a cell-nonautonomous regulator of stress resistance and longevity. *Cell* **153**, 1435–1447 (2013).
13. S. Imanikia *et al.*, Neuronal XBP-1 activates intestinal lysosomes to improve proteostasis in *C. elegans*. *Curr. Biol.* **29**, 2322–2338.e7 (2019).
14. S. Imanikia *et al.*, XBP-1 remodels lipid metabolism to extend longevity. *Cell Rep.* **28**, 581–589.e4 (2019).
15. P. M. Douglas *et al.*, Heterotypic signals from neural HSF-1 separate thermotolerance from longevity. *Cell Rep.* **12**, 1196–1204 (2015).
16. S. Nakamura *et al.*, Mondo complexes regulate TFEB via TOR inhibition to promote longevity in response to gonadal signals. *Nat. Commun.* **7**, 10944 (2016).
17. M. Sardiello *et al.*, A gene network regulating lysosomal biogenesis and function. *Science* **325**, 473–477 (2009).
18. C. Settembre *et al.*, TFEB links autophagy to lysosomal biogenesis. *Science* **332**, 1429–1433 (2011).
19. C. Settembre *et al.*, TFEB controls cellular lipid metabolism through a starvation-induced autoregulatory loop. *Nat. Cell Biol.* **15**, 647–658 (2013).
20. M. L. Toth *et al.*, Longevity pathways converge on autophagy genes to regulate life span in *Caenorhabditis elegans*. *Autophagy* **4**, 330–338 (2008).
21. L. R. Lapierre *et al.*, The TFEB orthologue HLH-30 regulates autophagy and modulates longevity in *Caenorhabditis elegans*. *Nat. Commun.* **4**, 2267 (2013).
22. M. V. Espelt *et al.*, Oscillatory Ca2+ signaling in the isolated *Caenorhabditis elegans* intestine: Role of the inositol-1,4,5-trisphosphate receptor and phospholipases C beta and gamma. *J. Gen. Physiol.* **126**, 379–392 (2005).
23. H. Qadota *et al.*, Establishment of a tissue-specific RNAi system in *C. elegans*. *Gene* **400**, 166–173 (2007).
24. A. Calixto *et al.*, Enhanced neuronal RNAi in *C. elegans* using SID-1. *Nat. Methods* **7**, 554–559 (2010).
25. D. B. Friedman, T. E. Johnson, A mutation in the age-1 gene in *Caenorhabditis elegans* lengthens life and reduces hermaphrodite fertility. *Genetics* **118**, 75–86 (1988).
26. K. D. Kimura *et al.*, daf-2, an insulin receptor-like gene that regulates longevity and diapause in *Caenorhabditis elegans*. *Science* **277**, 942–946 (1997).
27. M. L. Nonet *et al.*, *Caenorhabditis elegans* rab-3 mutant synapses exhibit impaired function and are partially depleted of vesicles. *J. Neurosci.* **17**, 8061–8073 (1997).
28. A. Dillin, D. K. Crawford, C. Kenyon, Timing requirements for insulin/IGF-1 signaling in *C. elegans*. *Science* **298**, 830–834 (2002).
29. M. E. Giannakou *et al.*, Dynamics of the action of dFOXO on adult mortality in Drosophila. *Aging Cell* **6**, 429–438 (2007).
30. Y. Volovik *et al.*, Temporal requirements of heat shock factor-1 for longevity assurance. *Aging Cell* **11**, 491–499 (2012).
31. D. Grushko *et al.*, Temporal requirements of SKN-1/NRF as a regulator of lifespan and proteostasis in *Caenorhabditis elegans*. *PLoS One* **16**, e0243522 (2021).
32. A. Ghaddar *et al.*, Whole-body gene expression atlas of an adult metazoan. *Sci. Adv.* **9**, eadg0506 (2023).
33. X. X. Lin *et al.*, DAF-16/FOXO and HLH-30/TFEB function as combinatorial transcription factors to promote stress resistance and longevity. *Nat. Commun.* **9**, 4400 (2018).
34. G. V. Clokey, L. A. Jacobson, The autofluorescent "lipofuscin granules" in the intestinal cells of Caenorhabditis elegans are secondary lysosomes. *Mech. Ageing Dev.* **35**, 79–94 (1986).
35. T. A. Forge, A. E. Macguidwin, Nematode autofluorescence and its use as an indicator of viability. *J. Nematol.* **21**, 399–403 (1989).
36. B. Gerstbrein *et al.*, In vivo spectrofluorimetry reveals endogenous biomarkers that report healthspan and dietary restriction in *Caenorhabditis elegans*. *Aging Cell* **4**, 127–137 (2005).
37. N. A. Swierczek *et al.*, High-throughput behavioral analysis in *C. elegans*. *Nat. Methods* **8**, 592–598 (2011).
38. M. D. McGee *et al.*, Loss of intestinal nuclei and intestinal integrity in aging *C. elegans*. *Aging Cell* **10**, 699–710 (2011).
39. S. Gelino *et al.*, Intestinal autophagy improves healthspan and longevity in *C. elegans* during dietary restriction. *PLoS Genet.* **12**, e1006135 (2016).
40. A. Meléndez *et al.*, Autophagy genes are essential for dauer development and life-span extension in *C. elegans*. *Science* **301**, 1387–1391 (2003).
41. M. Hansen *et al.*, A role for autophagy in the extension of lifespan by dietary restriction in *C. elegans*. *PLoS Genet.* **4**, e24 (2008).

42. L. R. Lapierre *et al.*, Autophagy and lipid metabolism coordinately modulate life span in germline-less *C. elegans*. *Curr. Biol.* **21**, 1507–1514 (2011).
43. S. Nakamura, T. Yoshimori, Autophagy and longevity. *Mol. Cells* **41**, 65–72 (2018).
44. C. Kang, Y. J. You, L. Avery, Dual roles of autophagy in the survival of *Caenorhabditis elegans* during starvation. *Genes. Dev.* **21**, 2161–2171 (2007).
45. J. F. Morley *et al.*, The threshold for polyglutamine-expansion protein aggregation and cellular toxicity is dynamic and influenced by aging in *Caenorhabditis elegans*. *Proc. Natl. Acad. Sci. U.S.A.* **99**, 10417–10422 (2002).
46. K. Jia, A. C. Hart, B. Levine, Autophagy genes protect against disease caused by polyglutamine expansion proteins in *Caenorhabditis elegans*. *Autophagy* **3**, 21–25 (2007).
47. A. M. Choi, S. W. Ryter, B. Levine, Autophagy in human health and disease. *N Engl. J. Med.* **368**, 651–662 (2013).
48. W. M. Winston, C. Molodowitch, C. P. Hunter, Systemic RNAi in *C. elegans* requires the putative transmembrane protein SID-1. *Science* **295**, 2456–2459 (2002).
49. S. G. Amara, A. C. Fontana, Excitatory amino acid transporters: Keeping up with glutamate. *Neurochem. Int.* **41**, 313–318 (2002).
50. B. I. Kanner, L. Borre, The dual-function glutamate transporters: Structure and molecular characterisation of the substrate-binding sites. *Biochim. Biophys. Acta* **1555**, 92–95 (2002).
51. I. Mano, S. Straud, M. Driscoll, *Caenorhabditis elegans* glutamate transporters influence synaptic function and behavior at sites distant from the synapse. *J. Biol. Chem.* **282**, 34412–34419 (2007).
52. A. C. Fontana, Current approaches to enhance glutamate transporter function and expression. *J. Neurochem.* **134**, 982–1007 (2015).
53. R. Bernards, Transcriptional regulation. Flipping the Myc switch. *Curr. Biol.* **5**, 859–861 (1995).
54. A. N. Billin *et al.*, MondoA, a novel basic helix-loop-helix-leucine zipper transcriptional activator that constitutes a positive branch of a max-like network. *Mol. Cell Biol.* **20**, 8845–8854 (2000).
55. C. L. Pickett, K. T. Breen, D. E. Ayer, A *C. elegans* Myc-like network cooperates with semaphorin and Wnt signaling pathways to control cell migration. *Dev. Biol.* **310**, 226–239 (2007).
56. B. R. Wilde, D. E. Ayer, Interactions between Myc and MondoA transcription factors in metabolism and tumourigenesis. *Br. J. Cancer* **113**, 1529–1533 (2015).
57. S. E. Celniker *et al.*, Unlocking the secrets of the genome. *Nature* **459**, 927–930 (2009).
58. S. Speese *et al.*, UNC-31 (CAPS) is required for dense-core vesicle but not synaptic vesicle exocytosis in *Caenorhabditis elegans*. *J. Neurosci.* **27**, 6150–6162 (2007).
59. J. M. Madison, S. Nurrish, J. M. Kaplan, UNC-13 interaction with syntaxin is required for synaptic transmission. *Curr. Biol.* **15**, 2236–2242 (2005).
60. M. C. Thein *et al.*, Combined extracellular matrix cross-linking activity of the peroxidase MLT-7 and the dual oxidase BLI-3 is critical for post-embryonic viability in *Caenorhabditis elegans*. *J. Biol. Chem.* **284**, 17549–17563 (2009).
61. H. Moribe *et al.*, Tetraspanin is required for generation of reactive oxygen species by the dual oxidase system in *Caenorhabditis elegans*. *PLoS Genet.* **8**, e1002957 (2012).
62. R. van der Hoeven *et al.*, Localization of the dual oxidase BLI-3 and characterization of its NADPH oxidase domain during infection of *Caenorhabditis elegans*. *PLoS One* **10**, e0124091 (2015).
63. C. Y. Ewald *et al.*, NADPH oxidase-mediated redox signaling promotes oxidative stress resistance and longevity through memo-1 in *C. elegans*. *Elife* **6**, e19493 (2017).
64. H. Sasakura *et al.*, Lifespan extension by peroxidase and dual oxidase-mediated ROS signaling through pyrroloquinoline quinone in *C. elegans*. *J. Cell Sci.* **130**, 2631–2643 (2017).
65. C. Y. Ewald, Redox signaling of NADPH oxidases regulates oxidative stress responses, immunity and aging. *Antioxidants (Basel)***7**, 130 (2018).
66. D. Harman, Aging: A theory based on free radical and radiation chemistry. *J. Gerontol.* **11**, 298–300 (1956).
67. B. D'Autreaux, M. B. Toledano, ROS as signalling molecules: Mechanisms that generate specificity in ROS homeostasis. *Nat. Rev. Mol. Cell Biol.* **8**, 813–824 (2007).
68. T. Finkel, Signal transduction by reactive oxygen species. *J. Cell Biol.* **194**, 7–15 (2011).
69. C. R. Reczek, N. S. Chandel, ROS-dependent signal transduction. *Curr. Opin. Cell Biol.* **33**, 8–13 (2015).
70. Y. Wei, C. Kenyon, Roles for ROS and hydrogen sulfide in the longevity response to germline loss in *Caenorhabditis elegans*. *Proc. Natl. Acad. Sci. U.S.A.* **113**, E2832–E2841 (2016).
71. D. Bazopoulou *et al.*, Developmental ROS individualizes organismal stress resistance and lifespan. *Nature* **576**, 301–305 (2019).
72. J. M. Van Raamsdonk, Levels and location are crucial in determining the effect of ROS on lifespan. *Worm* **4**, e1094607 (2015).
73. J. Tao *et al.*, Antioxidant response is a protective mechanism against nutrient deprivation in *C. elegans*. *Sci. Rep.* **7**, 43547 (2017).
74. J. H. Park *et al.*, Role of phospholipase D in the lifespan of *Caenorhabditis elegans*. *Exp. Mol. Med.* **50**, 1–10 (2018).
75. H. A. Miller *et al.*, Cell non-autonomous regulation of health and longevity. *Elife* **9**, e62659 (2020).
76. S. Q. Wong *et al.*, Neuronal HLH-30/TFEB modulates peripheral mitochondrial fragmentation to improve thermoresistance in Caenorhabditis elegans. *Aging Cell* **22**, e13741 (2023).
77. V. K. Mony *et al.*, Context-specific regulation of lysosomal lipolysis through network-level diverting of transcription factor interactions. *Proc. Natl. Acad. Sci. U.S.A.* **118**, e2104832118 (2021).
78. J. W. Olney, Brain lesions, obesity, and other disturbances in mice treated with monosodium glutamate. *Science* **164**, 719–721 (1969).
79. X. X. Dong, Y. Wang, Z. H. Qin, Molecular mechanisms of excitotoxicity and their relevance to pathogenesis of neurodegenerative diseases. *Acta Pharmacol. Sin* **30**, 379–387 (2009).
80. J. D. Rothstein *et al.*, Selective loss of glial glutamate transporter GLT-1 in amyotrophic lateral sclerosis. *Ann. Neurol.* **38**, 73–84 (1995).
81. S. Li *et al.*, Glutamate transporter alterations in Alzheimer disease are possibly associated with abnormal APP expression. *J. Neuropathol. Exp. Neurol.* **56**, 901–911 (1997).
82. C. P. Jacob *et al.*, Alterations in expression of glutamatergic transporters and receptors in sporadic Alzheimer's disease. *J. Alzheimers Dis.* **11**, 97–116 (2007).
83. M. L. Weller *et al.*, Selective overexpression of excitatory amino acid transporter 2 (EAAT2) in astrocytes enhances neuroprotection from moderate but not severe hypoxia-ischemia. *Neuroscience* **155**, 1204–1211 (2008).
84. Q. Kong *et al.*, Small-molecule activator of glutamate transporter EAAT2 translation provides neuroprotection. *J. Clin. Invest.* **124**, 1255–1267 (2014).
85. A. C. Todd, G. E. Hardingham, The regulation of astrocytic glutamate transporters in health and neurodegenerative diseases. *Int. J. Mol. Sci.* **21**, 9607 (2020).
86. J. V. Andersen *et al.*, Glutamate metabolism and recycling at the excitatory synapse in health and neurodegeneration. *Neuropharmacology* **196**, 108719 (2021).
87. S. Brenner, The genetics of *Caenorhabditis elegans*. *Genetics* **77**, 71–94 (1974).
88. S. Nakamura *et al.*, Suppression of autophagic activity by Rubicon is a signature of aging. *Nat. Commun.* **10**, 847 (2019).
89. T. Shioda, S. Nakamura, T. Yoshimori, Neuronal HLH-30 regulates glp-1 longevity independent of neuronal MML-1/MXL-2. NCBI Gene Expression Omnibus. https://www.ncbi.nlm.nih.gov/geo/query/acc.cgi?acc=GSE234429. Deposited 7 June 2023.
90. T. Shioda, S. Nakamura, T. Yoshimori, Neuronal MML-1/MXL-2 regulates autophagic and peroxidase activity via glutamate transporter to prolong lifespan. NCBI Gene Expression Omnibus. https://www.ncbi.nlm.nih.gov/geo/query/acc.cgi?acc=GSE234430. Deposited 7 June 2023.